# Extratropical Southern Hemisphere Synchronous Pressure Variability in the Early Twentieth Century

RYAN L. FOGT<sup>a</sup> AND CHARLOTTE J. CONNOLLY<sup>a</sup>

a Department of Geography and Scalia Laboratory for Atmospheric Analysis, Ohio University, Athens, Ohio

(Manuscript received 1 July 2020, in final form 20 April 2021)

ABSTRACT: Because continuous meteorological observations across Antarctica did not start until the middle of the twentieth century, little is known about the full spatial pattern of pressure variability across the extratropical Southern Hemisphere (SH) in the early twentieth century, defined here as the period from 1905 to 1956. To fill this gap, this study analyzes pressure observations across the SH in conjunction with seasonal pressure reconstructions across Antarctica, which are based on observed station-to-station statistical relationships between pressure over Antarctica and the southern midlatitudes. Using this newly generated dataset, it is found that the early twentieth century is characterized by synchronous but opposite-signed pressure relationships between Antarctica and the SH midlatitudes, especially in austral summer and autumn. The synchronous pressure relationships are consistent with the southern annular mode, extending its well-known influence on SH extratropical pressure since 1957 into the early twentieth century. Apart from connections with the southern annular mode, regional and shorter-duration pressure trends are found to be associated with influences from tropical variability and potentially the zonal wavenumber 3 pattern. Although the reduced network of SH observations and Antarctic reconstruction captures the southern annular mode in the early twentieth century, reanalysis products show varying skill in reproducing trends and variability, especially over the oceans and high southern latitudes prior to 1957, which stresses the importance of continual efforts of historical data rescue in data-sparse regions to improve their quality.

KEYWORDS: Antarctica; Pressure; Climate variability; Surface pressure; Decadal variability; Trends

### 1. Introduction

The dominant mode of atmospheric variability in the extratropical Southern Hemisphere (SH) on monthly and longer time scales is the southern annular mode (SAM) (Fogt and Marshall 2020). Associated with the intensity and north–south movement of the SH polar jet, in its positive phase the SAM is characterized by lower-than-average pressures/geopotential heights over Antarctica, and above average pressure/geopotential height in the SH midlatitudes (Rogers and van Loon 1982; Thompson and Wallace 2000). The increased equator to pole pressure gradient during positive SAM phases is also associated with an intensification and poleward movement of the polar jet, demonstrating a near synchronous, but opposing, response in pressure across much of the extratropical SH (Gillett et al. 2006).

Indices that monitor the SAM display positive and statistically significant trends in austral summer [hereinafter December–February (DJF)] since 1957, the start of the International Geophysical Year (IGY) when the majority of Antarctic observations begin. The DJF positive SAM trends, linked with negative pressure trends across Antarctica, have been primarily attributed to Antarctic stratospheric ozone depletion (Thompson and Solomon 2002; Polvani et al. 2011; Banerjee et al. 2020). In austral autumn [March–May (MAM)], the

Corresponding author: Ryan L. Fogt, fogtr@ohio.edu

are most likely consistent with internal variability (Fogt et al. 2009), with forcing from ozone depletion playing a secondary role (Thompson and Solomon 2002; Turner et al. 2009). In other seasons, the SAM has shown statistically nonsignificant trends since 1957 as a manifestation of strong decadal variability in extratropical pressure and the SH jet (Fogt and Marshall 2020). However, because most Antarctic observations do not exist prior to the start of the IGY in 1957/58 (Jones and Wigley 1988), the SAM variability in the early twentieth century is more complicated to understand. Without continuous measurements of the high southern latitude component of the SAM prior to the IGY, challenges remain in analyzing the large-scale SH atmospheric circulation in the early twentieth century (Carleton 2003). Nonetheless, a few published SAM reconstructions that extend back to 1905 or earlier suggest the recent trends since 1957 in DJF are unique in the last century (Jones and Widmann 2003, 2004; Fogt et al. 2009, 2017) and through the last millennium (Abram et al. 2014).

SAM has also displayed positive trends since the 1960s, which

As a result of longer observational datasets, more is known prior to the IGY about the seasonal and interannual mid-latitude component of SH atmospheric circulation across Australia, New Zealand, South America, and South Africa as discussed in earlier work (Jones 1991; Allan et al. 1995; Karoly et al. 1996; Alexander et al. 2010). To connect these observations before 1957 poleward to Antarctica, reconstructions from ice cores and snow pits can add value, although the circulation changes from these proxy measurements usually only have a regional signature, and they often cannot resolve changes across the seasons (Enomoto 1991; Kreutz et al. 2000; Souney 2002; Goodwin et al. 2004; Xiao et al. 2004; Russell and

<sup>©</sup> Supplemental information related to this paper is available at the Journals Online website: https://doi.org/10.1175/JCLI-D-20-0498.s1.

McGregor 2010; Dixon et al. 2012; Bracegirdle et al. 2019). Other studies examining the transpolar index (TPI)—the difference in normalized pressures between Hobart, Tasmania, Australia, and Stanley, Falkland Islands (Pittock 1980)—similarly provide additional knowledge on regional SH extratropical pressure relationships prior to the IGY because observations at both Hobart and Stanley exist throughout the twentieth century; a tree-ring-based reconstruction has farther extended the summer TPI record back into the late eighteenth century (Villalba et al. 1997). Like much research using proxy measurements from Antarctica, these studies hint that synchronous opposing pressure relationships (seesaws) have existed throughout the twentieth century. However, the strength of this relationship varies in time (Villalba et al. 1997), and the TPI primarily represents an atmospheric state characterized by one large ridge and trough across the SH (zonal wavenumber 1). Furthermore, the TPI may miss patterns associated with the more generally zonally symmetric SAM or other modes of extratropical atmospheric circulation variability (Jones et al. 1999). To move beyond the regional relationships captured by the TPI or Antarctic proxy measurements, a more complete view encompassing the meteorological observational network across Antarctica is gained by using Antarctic station-based pressure reconstructions (Fogt et al. 2016a,b, 2017) throughout the twentieth century. Like the TPI, comparisons between these pressure reconstructions in atmosphere-only climate models, which are constrained at their lower boundary and therefore have an overall realistic depiction of SH pressure variability (Fogt et al. 2017; Schneider and Fogt 2018; Fogt et al. 2019), also hint at the stable pressure relationships between the middle and high latitudes of the SH since 1905 (Clark and Fogt 2019).

This study builds upon these previous studies and aims to improve the understanding of synchronous extratropical SH pressure variability throughout the entire twentieth century. By combining observations in the SH midlatitudes with observationally based pressure reconstructions over Antarctica, this study provides the best estimate to date of seasonally resolved and spatially complete extratropical SH pressure variability in the early twentieth century, defined here as the period from 1905 to the IGY, especially outside the Antarctic Peninsula.

### 2. Data and methods

We analyze a combination of pressure observations from 30 long-term stations across the extratropical SH (Table 1) along with 17 Antarctic stations of merged seasonal pressure reconstructions (Fogt et al. 2016a) with Antarctic observations (Table 2) to provide a continuous estimate of extratropical SH pressure variability from 1905 to 2018 (Fig. 1). For the midlatitude observations (stations 1–30 in Fig. 1), the primary source of data is the University Corporation for Atmospheric Research research data archive dataset 570.0, which contains quality-controlled monthly mean surface and/or sea level pressure globally from 1738 to the present. We use only land-based measurements from this dataset, although the archive includes other observations as well. To provide the most

complete continuous records, missing data were patched for a few stations using neighboring observations based on mean differences during the period of overlap; the patching is relatively minor as only the most complete stations were initially selected. For pressure at Tahiti, French Polynesia, we use data from the Australian Bureau of Meteorology/Météo France (ftp://ftp.bom.gov.au/anon/home/ncc/www/sco/soi/tahitimslp.html) because it is more complete throughout the twentieth century than other records for this station (Allan et al. 1991; Ropelewski and Jones 1987). Data at Stanley on the Falkland Islands are extended with a nearby station, although there is still a gap from 1982 to 1991. Further details for these SH midlatitude observations are listed in Table 1.

For the Antarctic data (stations 31–47 in Fig. 1), we merge seasonal means calculated from observations (after they begin, see start date in Table 2) with seasonal mean pressure reconstructions (Fogt et al. 2016a, 2019). In DJF, we use the original reconstructions for each station, which are calculated using a principal component regression model that is based solely on statistical relationships between midlatitude pressure and the Antarctic station that is reconstructed. For all other seasons [austral autumn, MAM; austral winter, June-August (JJA); and austral spring, September-November (SON)], we make use of the so-called pseudoreconstructions, in which the principal component regression model to create the pressure reconstruction also includes estimates extracted from a gridded pressure dataset at key points over the ocean, in addition to midlatitude pressure observations. The addition of the ocean gridpoint data as predictors in the reconstruction model markedly increases its skill outside the austral summer (Fogt et al. 2016a). Spatially, the station-based reconstructions align best with observations along the Antarctic Peninsula in all seasons but have correlations with the observations above 0.6; the skill is considerably higher in DJF. In subsequent work, these pressure reconstructions at various Antarctic stations were interpolated using a kriging technique to produce a spatially complete seasonal reconstruction poleward of 60°S (Fogt et al. 2019). The skill of this spatially complete reconstruction broadly follows that of the station-based reconstructions, and when compared with independent observations from ships and early Antarctic expeditions, the bias of 2-4 hPa determined after 1979 (smaller in summer) is still observed prior to 1979 (Fogt et al. 2020). Further details of the Antarctic station-based pressure reconstructions can be found in earlier work (Fogt et al. 2016a,b, 2017, 2019) and in Table 2.

Gridded pressure data from a suite of twentieth-century reanalyses are also used for further comparison. These consist of the National Oceanic and Atmospheric Administration (NOAA)/Cooperative Institute for Research in Environmental Sciences Department of Energy twentieth century reanalysis, version 3 (20CRv3) (Slivinski et al. 2019), the European Centre for Medium-Range Weather Forecasts (ECMWF) twentieth-century reanalysis (ERA-20C) (Poli et al. 2016), and ECMWF's coupled ocean—atmosphere reanalysis of the twentieth century (CERA-20C) (Laloyaux et al. 2018). All of these twentieth-century reanalyses primarily assimilate only surface pressure observations; ERA-20C and CERA-20 also assimilate marine surface winds, and CERA-20 further assimilates ocean

TABLE 1. Information on the pressure observations used in this study. The South African stations were patched with monthly mean pressure data calculated from the National Centers for Environmental Information (NCEI) dataset Global Surface Summary of the Day (https://data.nodc.noaa.gov/cgi-bin/iso?id=gov.noaa.ncdc:C00516#). Note that data for Stanley were extended from 1991 to 2018 using nearby station 888890.

Station name	Lat	Lon	Station ID	Start year	End year	Percent complete	Patched station ID
Cape Town	34.0°S	18.6°E	688160	1841	2018	99.53	NCEI 688160
Port Elizabeth	34.0°S	25.6°E	688420	1887	2018	99.81	NCEI 688420
Durban	30.0°S	31.0°E	685880	1884	2018	99.01	NCEI 685880
Perth	31.9°S	116.0°E	946100	1876	2018	99.83	_
Alice Springs	23.8°S	133.9°E	943260	1885	2018	99.56	_
Adelaide	35.0°S	138.5°E	946720	1857	2018	99.69	_
Melbourne	37.8°S	145.0°E	948680	1903	2018	99.93	948650
Hobart	42.8°S	147.5°E	949750	1866	2018	96.46	_
Sydney	33.9°S	151.2°E	947680	1859	2018	99.32	947670
Brisbane	27.4°S	153.1°E	945780	1887	2018	99.94	_
Auckland	37.0°S	174.8°E	931190	1863	2018	77.44	933090
Hokitika	42.7°S	171.0°E	936150	1866	2018	91.34	936140
Dunedin	45.9°S	170.5°E	938940	1864	2018	99.14	5397
Christchurch	43.5°S	172.5°E	937800	1864	2018	98.66	937810
Wellington	41.3°S	174.8°E	934340	1864	2018	99.35	934170/936780
Chatham Island	44.0°S	176.6°W	939870	1878	2018	98.82	945760
Catamarca	28.6°S	65.8°W	872220	1901	2018	98.73	873450
Santiago	33.4°S	70.8°W	855740	1861	2018	99.74	_
Valdivia	39.6°S	73.1°W	857660	1899	2018	99.44	857430
Punta Arenas	53.0°S	70.8°W	859340	1889	2018	99.68	_
Sarmiento	45.6°S	69.1°W	878490	1903	2018	98.78	878600
Bahia Blanca	38.7°S	62.2°W	877500	1896	2018	97.97	_
Buenos Aires	34.6°S	58.5°W	875850	1858	2018	99.02	875760
Cordoba	31.3°S	64.2°W	873440	1873	2018	99.77	_
Rio de Janeiro	22.9°S	43.2°W	837430	1851	2018	99.36	837810
Stanley	51.0°S	57.0°W	999006	1900	1982	98.80	888900
•				1991	2018	87.36	888890
Orcadas	60.7°S	44.7°W	889680	1903	2018	99.57	_
Grytviken	54.0°S	36.0°W	889030	1905	2018	91.52	_
Tahiti	17.6°S	149.6°W	919380	1876	2018	100.00	_
St. Helena island	16.0°S	5.7°W	619010	1892	2018	99.28	_

temperature and salinity measurements. Because very few surface pressure observations prior to the IGY are located poleward of 60°S, the quality of these datasets diminishes before the mid-twentieth century (Schneider and Fogt 2018).

To improve the global estimate of pressure prior to the IGY, the Fogt et al. (2019) spatially complete pressure reconstruction was merged with 20CRv3 (at 1° × 1° latitude-longitude resolution) using a sine-based latitude weighting over the region 55°-65°S (poleward of 65°S, the reconstruction is used while 20CRv3 is used everywhere north of 55°S). In a 5° latitude-longitude region surrounding Orcadas near the Antarctic Peninsula (Fig. 1), the spatial reconstruction is used entirely because it is based on the observations from this station (dating back to 1903; Zazulie et al. 2010), which may not have always been assimilated into 20CRv3. The reconstruction is then blended into 20CRv3 over the adjacent 5° near Orcadas on the eastern, northern, and western edges using a similar sine-weighting. This dataset hereinafter is called the "merged" data, representing a spatially continuous pressure estimate that matches the station-based reconstructions over Antarctica from Fogt et al. (2016a, 2019) and the assimilated midlatitude data in 20CRv3 elsewhere. It is important to note that the merged data have not been forced to conserve atmospheric mass or any other property and are only meant to be employed here as another spatially complete estimate of pressure variability, particularly prior to IGY as the quality of gridded pressure datasets improves after 1957 with the inclusion of Antarctic data (Fogt et al. 2018; Schneider and Fogt 2018).

To investigate the connection of modes of climate variability with SH extratropical pressure throughout the twentieth century we employ several long-term indices. First, the "Fogt" seasonal SAM index reconstructions (Fogt et al. 2009; Jones et al. 2009), which extend back to at least 1905, are merged with the observationally based SAM index (Marshall 2003) after 1957 to depict changes and trends in this leading mode of SH extratropical climate variability throughout the twentieth century. To monitor fluctuations in El Niño-Southern Oscillation (ENSO), we use the Southern Oscillation index (SOI), the difference in standardized pressure from Tahiti, French Polynesia, and Darwin, Australia. We specifically use the SOI from the Australian Bureau of Meteorology because it does not have any gaps in the twentieth century (http://www.bom.gov.au/climate/current/soihtm1.shtml). For decadal-scale tropical variability, we also investigate the relationship of SH extratropical pressure with the unfiltered tripole index of the interdecadal Pacific oscillation (IPO)

TABLE 2. Information on the Antarctic station observations that were merged with the station-based pressure reconstructions. The starting and ending years and the percent-complete values given are for the observational record and not the reconstruction (which is complete from 1905 to 2013). Here, ID indicates the station identifier.

Station name	Lat	Lon	Station ID	Start year	End year	Percent complete
Novolazarevskaya	70.8°S	11.8°E	895120	1961	2018	99.43
Syowa	69.0°S	39.6°E	895320	1957	2018	91.13
Mawson	67.6°S	62.9°E	895640	1954	2018	99.49
Davis	68.6°S	78.0°E	895710	1957	2018	92.34
Mirny	66.6°S	93.0°E	895920	1956	2018	99.60
Vostok	78.5°S	106.9°E	896060	1958	2018	97.27
Casey	66.3°S	110.6°E	896110	1960	2018	98.79
Dumont d'Urville	66.7°S	140.0°E	896420	1956	2018	95.63
McMurdo/Scott Base	77.9°S	166.7°E	896640	1956	2012	97.75
Amundsen-Scott	90.0°S	$0.0^{\circ}\mathrm{E}$	890090	1957	2018	100.00
Byrd	80.0°S	119.4°W	893240	1957	2011	85.62
Rothera	67.6°S	68.1°W	890620	1946	2018	91.21
Faraday	65.3°S	64.3°W	890630	1950	2018	95.02
Bellingshausen	62.2°S	58.9°W	890500	1968	2018	99.86
Esperanza	63.4°S	57.0°W	889630	1945	2018	95.37
Marambio	64.2°S	56.7°W	890550	1970	2018	98.13
Halley	75.5°S	26.7°W	890220	1956	2018	98.54

(Henley et al. 2015), which is calculated using the difference of sea surface temperature anomalies averaged in the central equatorial Pacific, the northwest Pacific, and the southwest Pacific. The ENSO signal is linearly removed from the unfiltered IPO index and called the "IPO residual" throughout in order to examine decadal tropical variability independent of ENSO. Last, we also examine the zonal wavenumber 3 (ZW3) index (Raphael 2004), determined from SLP anomalies in three centers along 49°S using 20CRv3. Throughout our analysis, the statistical significance of trends, correlations, or between means is estimated using a *t* distribution, with the degrees of freedom reduced by the lag-1 autocorrelation (Bretherton et al. 1999). All data were detrended before performing any correlation analyses.

#### 3. Results

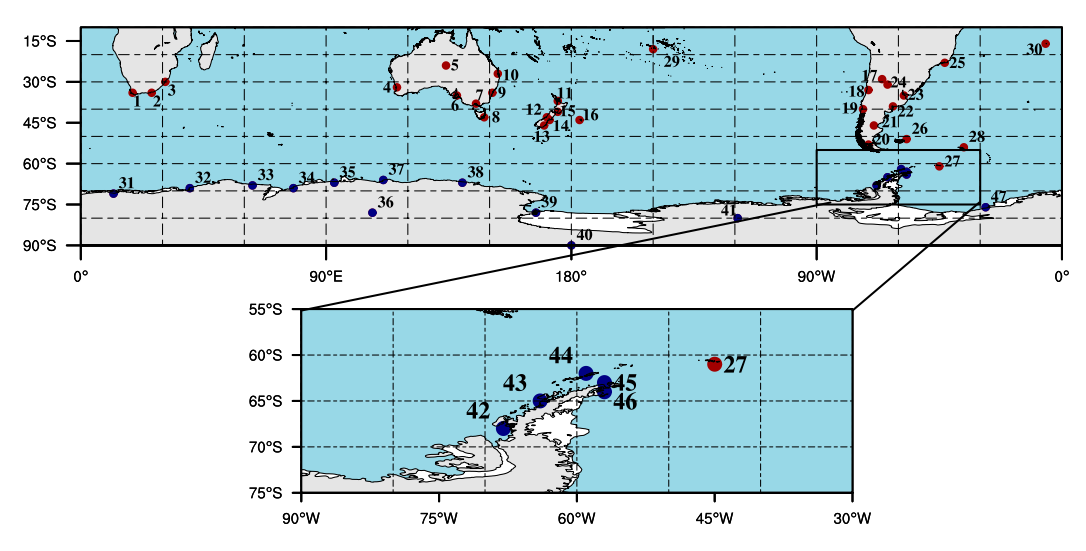
### a. Twentieth-century SH extratropical pressure trends

Thirty-year running pressure trends at the station locations (Fig. 1) for each season are displayed in Fig. 2. The negative pressure trends in Antarctica since the 1960s (especially away from the Antarctic Peninsula; Figs. 2a,b) are balanced by significant pressure increases in the midlatitudes, especially across much of Australia and South America. Importantly, Fig. 2 demonstrates that this synchronous pressure relationship between Antarctica and the SH midlatitudes extends throughout the early twentieth century. In the early twentieth century during DJF (Fig. 2a), significant pressure increases across much of coastal East Antarctica (Fogt et al. 2017) are offset by negative pressure trends throughout much of the SH midlatitudes, although only a few SH midlatitude observations show significant negative pressure trends. This connection is even stronger in MAM for 30-yr periods beginning in 1920-30 (Fig. 2b), where significant pressure increases across much of continental (non-peninsular) Antarctica prior to 1950 are offset by statistically significant negative pressure trends throughout much of South Africa, Australia, and New Zealand, as well as a few stations in South America. Indeed, in MAM the strongest negative pressure trends throughout the twentieth century in the SH midlatitudes correspond to the period of strongest positive pressure trends everywhere in Antarctica except the Antarctic Peninsula. Similar synchronous pressure relationships between Antarctica and the SH midlatitudes are also observed in JJA and SON prior to the IGY (Figs. 2c,d). Because the statistical model used to create the Antarctic pressure reconstructions was calibrated on detrended data after 1957, the existence of these synchronous relationships in the early twentieth century prior to 1957 is a reflection of the inherent SH extratropical spatial pressure covariance.

Apart from the dominant synchronous nature of SH extratropical pressure variability, the Antarctic pressure reconstructions and midlatitude pressure observations also show times of regional variability and trends in the early twentieth century. For example, in DJF most stations in New Zealand observe significant pressure increases throughout the mid-twentieth century (30-yr periods beginning in 1925-45) while there are significant negative pressure trends in South Africa; at this same time, there are only a few stations in the Ross Sea sector (Vostok-Byrd) that display significant negative pressure trends in the reconstructions across Antarctica (Fig. 2a). Further, the Antarctic Peninsula often has weaker pressure trends than the rest of Antarctica or, as in the case in MAM, much stronger and significant positive pressure trends in the late twentieth century (30-yr periods beginning in 1955-65). The regional and independent character of these trends suggests that other processes besides the SAM are also important for early twentieth-century pressure variability across the extratropical SH; these relationships will be explored in more detail in section 3c.

To provide a spatially complete perspective, pressure trends in the early twentieth century from various gridded datasets

### **Observation and Reconstruction Locations**



### **Pressure Observations**

1. Cape Town	6. Adelaide	11. Auckland	16. Chatham Island	21. Sarmiento	26. Stanley
2. Port Elizabeth	7. Melbourne	12. Hokitika	17. Catamarca	22. Bahia Blanca	27. Orcadas
3. Durban	8. Hobart	13. Dunedin	18. Santiago	23. Buenos Aires	28. Grytviken
4. Perth	9. Sydney	14. Christchurch	19. Valdivia	24. Cordoba	29. Tahiti
5. Alice Springs	10. Brisbane	15. Wellington	20. Punta Arenas	25. Rio de Janeiro	30. St. Helena Island

### **Antarctic Pressure Reconstructions & Observations**

31. Novolazarevskaya 32. Syowa	36. Vostok 37. Casev	40. Amundsen Scott 41. Byrd	44. Bellingshausen 45. Esperanza
33. Mawson	38. Dumont d'Urville	42. Rothera	46. Marambio
34. Davis	39. McMurdo / Scott Base	43. Faraday	47. Halley

FIG. 1. Map of the midlatitude station observations (numbers 1–30, plotted in red) and the merged Antarctic pressure reconstructions and observations (numbers 31–47, plotted in blue) used in the study. A zoomed map of the Antarctic Peninsula region is provided for more detail. Stations are numbered approximately from east to west within each group, except for the subtropical island stations (29–30), which are the last of the midlatitude group.

are plotted for DJF and MAM in Fig. 3, along with the observation and reconstruction trends. In the SH midlatitudes, the gridded datasets match the observed trends to varying degrees, with the best match in terms of magnitude and statistical significance perhaps coming from 20CRv3. Poleward of 60°S, however, 20CRv3, ERA-20C, and CERA-20C all produce significant negative trends, which do not reflect the reconstructions, even along the Antarctic Peninsula (where there are nearby observations in the early twentieth century; Fig. 1). The negative trends are especially large in ERA-20C, which can have biases of more than 10 hPa relative to the reconstructions (Schneider and Fogt 2018; Fogt et al. 2019).

Although not dynamically constrained, the merged data provide a more likely estimate of the spatially complete pressure variability across the extratropical SH (Fig. 3a). This dataset shows the significant positive pressure increases across much of East Antarctica and the Antarctic interior in DJF and MAM (Fogt et al. 2017, 2019), which are largely offset by pressure decreases across much of the SH midlatitudes (indicated by the observations; Figs. 2 and 3). The significant positive pressure trends depicted in the tropical and subtropical SH Pacific Ocean

in 20CRv3 (and thus, the merged data) do not match the observations at Tahiti, which show much weaker and statistically insignificant pressure increases. Therefore, it is likely that there are even more widespread negative pressure trends in DJF across much of the SH midlatitudes, again reflecting the synchronous pressure variability throughout the extratropical SH in the early twentieth century prior to the IGY. A similar story is also seen in MAM, although because the significant negative trends are generally shorter in duration than in DJF (Fig. 2), the synchronous relationship is not fully depicted in the spatial trends from 1905–56.

Spatial trend maps for JJA and SON in the early twentieth century are plotted in Fig. 4. Most readily apparent in these seasons are the large differences between the reanalyses poleward of 60°S (Schneider and Fogt 2018) especially ERA-20C in SON (Fig. 4c) and CERA-20C in JJA (Fig. 4d). Although a strong synchronous opposite-signed pressure relationship is suggested by ERA-20C, these trends and their significance do not align with the observations or the reconstructions, suggesting that this relationship is artificial. While the merged data suggest a synchronous relationship in these seasons (Fig. 4a),

### 30-yr Running Station Trends

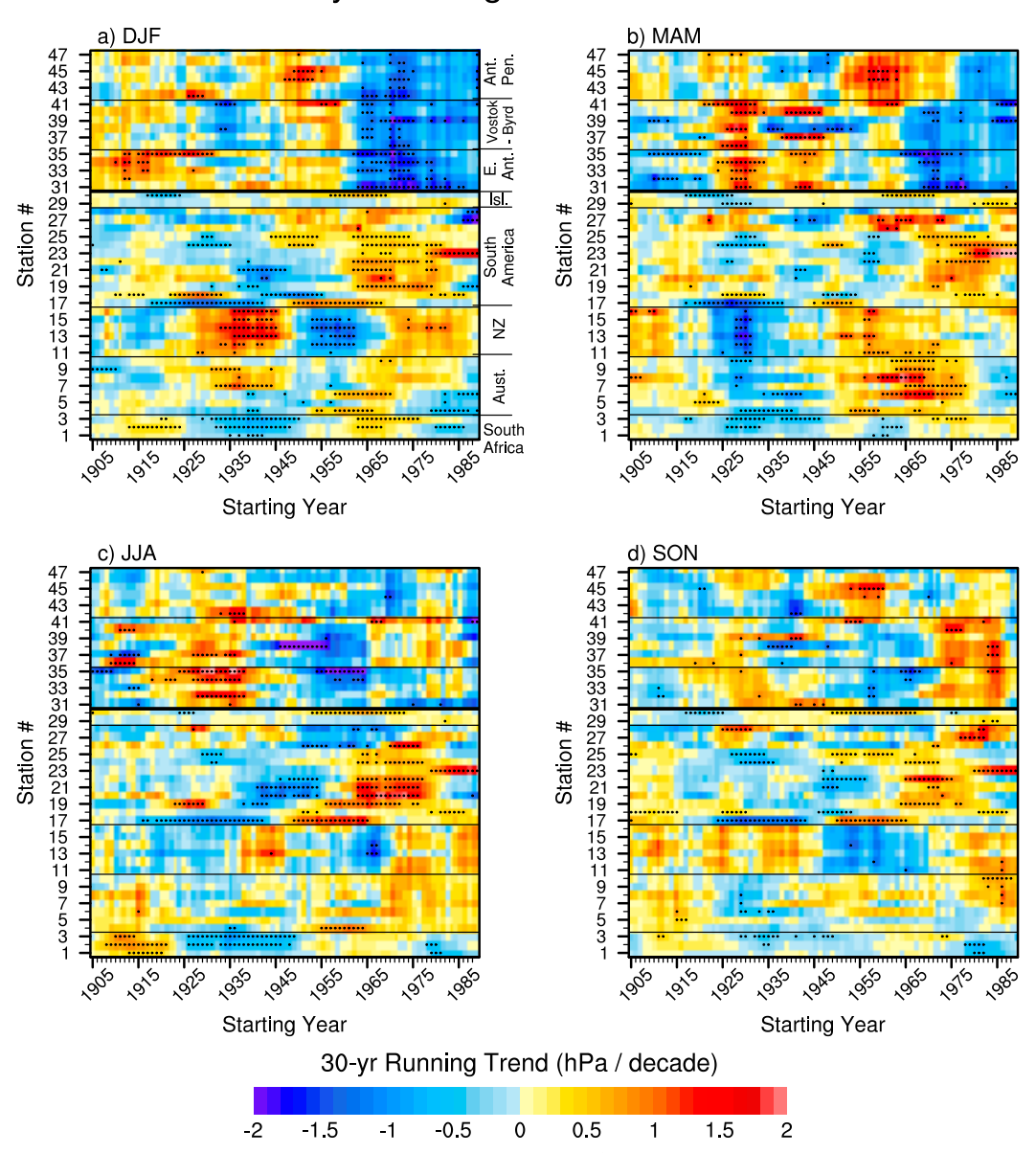


FIG. 2. The 30-yr running seasonal pressure trends (hPa decade<sup>-1</sup>), for (a) DJF, (b) MAM, (c) JJA, and (d) SON, with the station numbers on the y axis corresponding the station numbers in Fig. 1 and grouped with labels in the top-left panel (Aust. = Australia, NZ = New Zealand region, Isl. = subtropical islands, E. Ant = coastal East Antarctica; Vostok-Byrd = Antarctic stations east from Vostok to Byrd, and Ant. Pen. = stations near the Antarctic Peninsula). The x axis is the starting year for the 30-yr trend, and trends significantly different from zero at p < 0.05 are marked with a dot.

the trends are more regional. The less zonally symmetric structure to the pressure trends in JJA and SON is perhaps related to the more asymmetrical structure of the SAM in these seasons (Fogt et al. 2012), which ties to seasonal variations in the SH jet streams, and in particular the stronger subtropical jet in austral winter (Bals-Elsholz et al. 2001; Fogt and Marshall 2020), which tends to weaken the Pacific structure of the polar or midlatitude jet (Fogt et al. 2012). Additionally in both JJA and

SON, tropical teleconnections associated with ENSO variability are stronger, associated with a stronger Rossby wave source from the well-defined subtropical jet (Karoly 1989; Turner 2004; Yuan et al. 2018).

### b. SH extratropical pressure patterns prior to the IGY

To further analyze the spatial pressure relationships across the data represented in Figs. 3 and 4, empirical orthogonal

### Pressure Trend 1905-1956

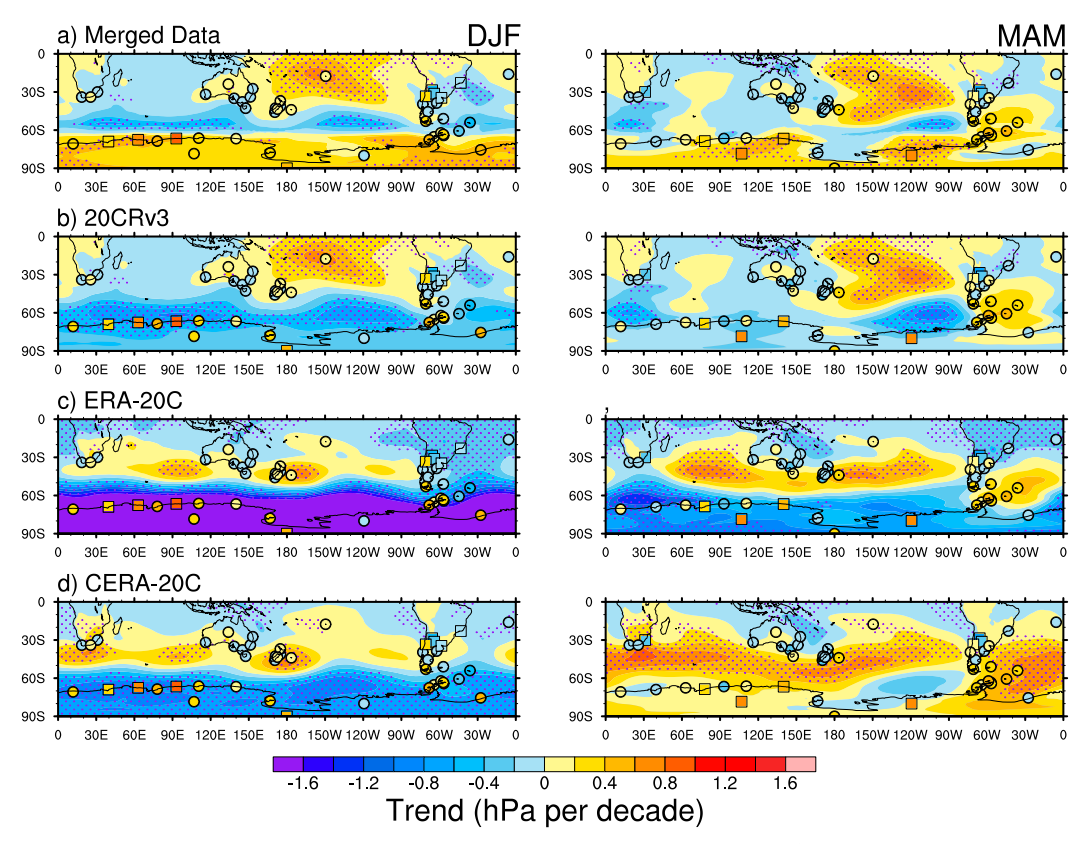


FIG. 3. Spatial seasonal [(left) DJF; (right) MAM] pressure SH trend (hPa decade<sup>-1</sup>) maps from gridded datasets (shading) and observations and reconstructions (symbols) for (a) merged reconstruction/20CRv3, (b) 20CRv3, (c) ERA-20C, and (d) CERA-20C. Trends significantly different from zero at p < 0.05 are stippled for the gridded datasets and plotted as squares for observations or reconstructions.

function (EOF) analysis is performed on the seasonal mean station data and Antarctic reconstructions in Fig. 2 as well as 20CRv3 and the merged data during 1905-56. The EOF analysis determines independent patterns of variability within each dataset prior to the IGY, and a principal component time series represents the amplitudes of these patterns through time. EOFs are calculated only for the first three leading patterns of variability as these represent approximately 50% or more of the total pressure variation within each dataset, and are often associated with leading modes of climate variability such as the SAM or ENSO (Thompson and Wallace 2000; Mo and Paegle 2001; Fogt and Bromwich 2006). For station observations and the Antarctic pressure reconstructions, the EOFs are based on standardized pressure at each location, where data that are still missing after patching are replaced with the station climatological means. For 20CRv3 and the merged data, EOFs are based on weighted (by cosine of latitude) MSLP (for 20CRv3) and surface pressure (for the merged data) data from 20° to 90°S. Principal component (PC) time series of the first three modes for these datasets are shown in Fig. 5; the PCs are inverted where necessary to make the correlations positive because the sign of the EOFs is arbitrary.

The station network, although spatially discrete (Fig. 1), is able to capture the EOF1/PC1 well, with correlations between PC1 of the merged and station data above 0.75. For all but 20CRv3 in MAM, PC1 is the highest correlated with the Fogt SAM reconstruction and thus depicts this mode of variability. In MAM, the low correlation between 20CRv3 and the merged data (Fig. 5b) reflects a different ordering of the EOFs: the SAM structure does not appear until EOF3 in 20CRv3, despite this being the dominant mode in reanalysis data in all seasons after 1979 (Fogt and Marshall 2020). The correlations with the station network and PC2/PC3 are smaller because the EOF patterns for these modes are more regional in character with larger loadings over the Pacific Ocean (not shown), and the spatially discrete station network does not reproduce these. Overall, the EOFs/PCs demonstrate that 20%–30% (>40% in summer) of the early twentieth-century SH extratropical variability is in EOF1, which shows synchronous opposite-signed pressure variability akin to the SAM in all seasons (Fig. 5), consistent with findings of the SAM/EOF1 after 1979 (Fogt and Marshall 2020). Furthermore, neither the station data nor the merged data show significant (p < 0.05) trends in PC1 in the early twentieth century in any season, whereas 20CRv3 shows

### Pressure Trend 1905-1956

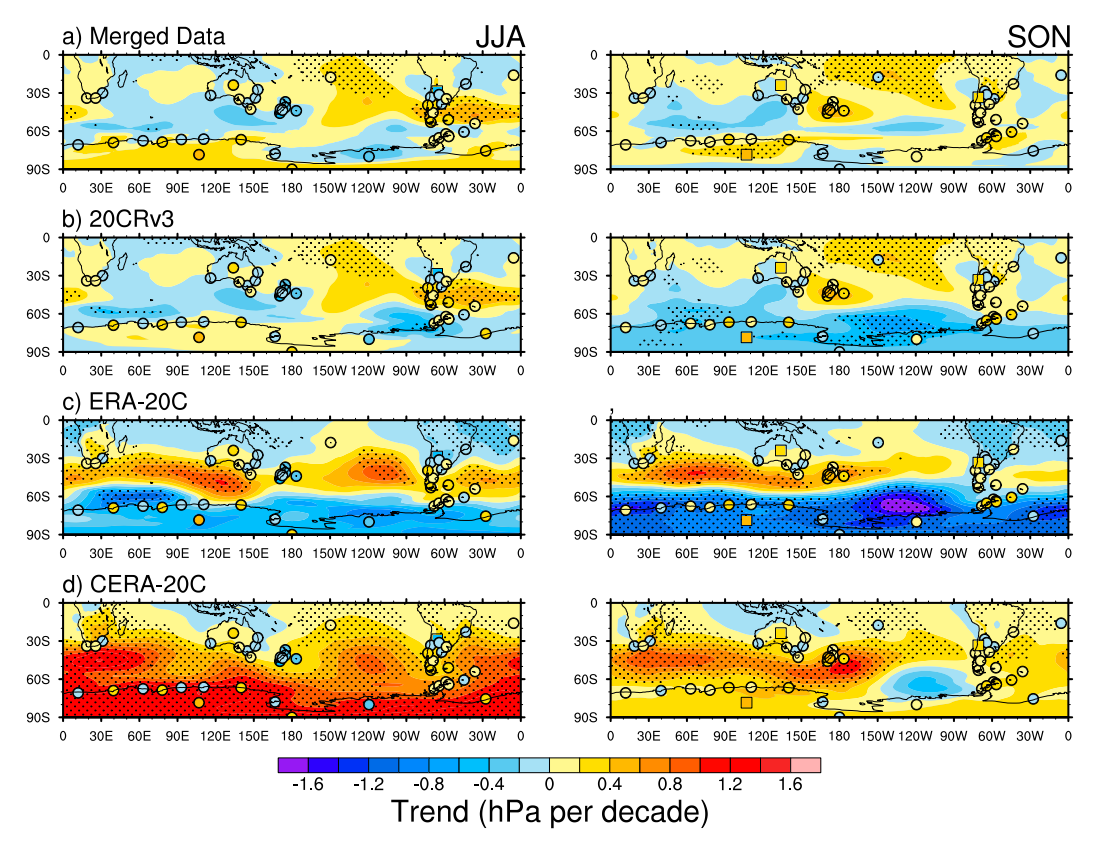


FIG. 4. As in Fig. 3, but for (left) JJA and (right) SON.

significant trends for PC1 in both DJF (Fig. 5a) and SON (Fig. 5d). The lack of significant trends in PC1/EOF1 in the early twentieth century is consistent with SAM reconstructions, which show the distinctiveness of the recent positive summer SAM index trends since the IGY (Jones et al. 2009; Abram et al. 2014; Dätwyler et al. 2018). For the other PCs, the trends are also often not significant in the early twentieth century, although all datasets suggest significant trends in PC2 during DJF (Fig. 5a).

## c. Pressure relationships with modes of climate variability prior to the IGY

To provide an overview of the general connections of SH extratropical pressure variability prior to the IGY with dominant modes of climate variability, Fig. 6 displays the 30-yr running trends from regionally averaged pressure from station groups in Fig. 2, along with the 30-yr running trends of the SAM reconstructions and extended with the observationally based SAM index, the SOI, the residual unfiltered tripole IPO index, and the ZW3 index. Prior to the regional averaging, all data are converted to anomalies by removing the 1905–2018 mean for each station. The use of anomalies ensures that averaging sea level and surface pressure observations together does not influence the results. Vertical lines in Fig. 6 depict

shifts in the SOI (solid vertical lines) and IPO (dashed vertical lines), determined from where the 30-yr running trends in these indices averaged across all seasons change sign and remain in that new phase for at least five continuous years. Recall the IPO index used in our analysis ("IPO residual") has the ENSO signal linearly removed to depict low-frequency Pacific oceanic variability across both the Northern and Southern Hemispheres independent from ENSO.

Consistent with the depiction in Figs. 3-5, Fig. 6 demonstrates that much of the synchronous SH extratropical pressure variability and trends throughout the entire twentieth century and to present are associated with the SAM. Even when there are nonsignificant SAM index trends (which is the case for much of the twentieth century), negative SAM index trends are typically associated with widespread positive pressure trends across Antarctica and negative pressure trends across the SH midlatitudes in all seasons. Similarly, positive SAM index trends are usually associated with pressure decreases across Antarctica and pressure increases across the majority of the midlatitudes. The strong synchronous pressure relationship in MAM from Fig. 2b discussed previously is one clear example: the significant (p < 0.05) negative SAM index trends from the 30-yr period starting in 1920-30 are associated with significant (p < 0.05) positive pressure trends across Antarctica (except

### Seasonal PC Timeseries 1905-1956

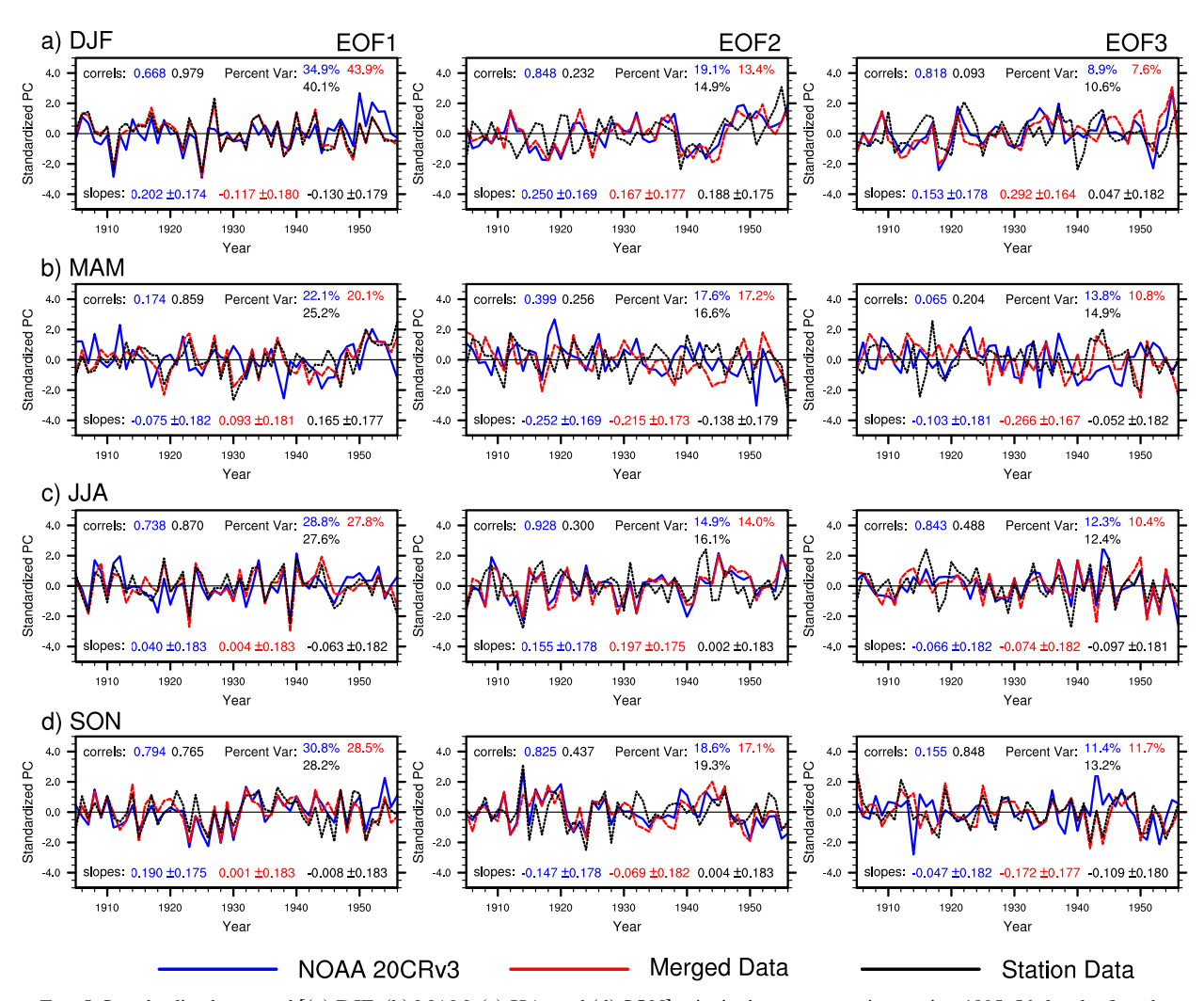


FIG. 5. Standardized seasonal [(a) DJF, (b) MAM, (c) JJA, and (d) SON] principal component time series, 1905–56, for the first three EOFs [(left) EOF1, (center) EOF2, and (right) EOF3] of NOAA 20CRv3 MSLP (blue), merged surface pressure data (red), and station observations and Antarctic reconstructions (black) from Fig. 1. The correlations with the merged data ("correls") as well as the percent variance explained ("Percent Var") and slopes (standard deviation per decade) are given in each panel, using the colors to represent each dataset. The PCs were inverted where necessary to make the correlations positive.

the Antarctic Peninsula), and significant negative pressure trends in New Zealand, Australia, and South Africa. This pattern of synchronous SH pressure variability associated with the SAM is also seen prior to the IGY in DJF, JJA, and SON. The dominance of the SAM signal connecting the middle and high latitudes of the SH both prior to and after the IGY is confirmed by pressure anomaly composites using the merged data based on the SAM index, provided in the online supplemental material (see Figs. S1 and S2 there). However, there are other possible teleconnections with different climate modes on different time scales, which operate more regionally. To aid in interpreting the regional connections, pressure anomaly composites using the merged data for strong positive and negative phases of the various climate indices prior to the IGY are also displayed in

Figs. 7–9. For completeness, we provide composites using the merged data for the period 1957–2013 for the other climate indices described in the remainder of this paper in Figs. S3–S5 of the online supplemental material.

### 1) RELATIONSHIPS WITH ENSO VARIABILITY

Tropical Pacific regime shifts associated with changes in the SOI/ENSO are depicted in Fig. 6 with solid vertical lines, corresponding roughly to 1925/26, 1952/53, and 1976/77. Although complex and varying by season, these regime shifts often correspond to fluctuations in the sign of 30-yr running pressure trends across South Africa, Australia, New Zealand, and the Antarctic Peninsula prior to the IGY. The ENSO composites in Fig. 7 further depict some of these relationships, with the

### 30-yr Running Trends Comparisons

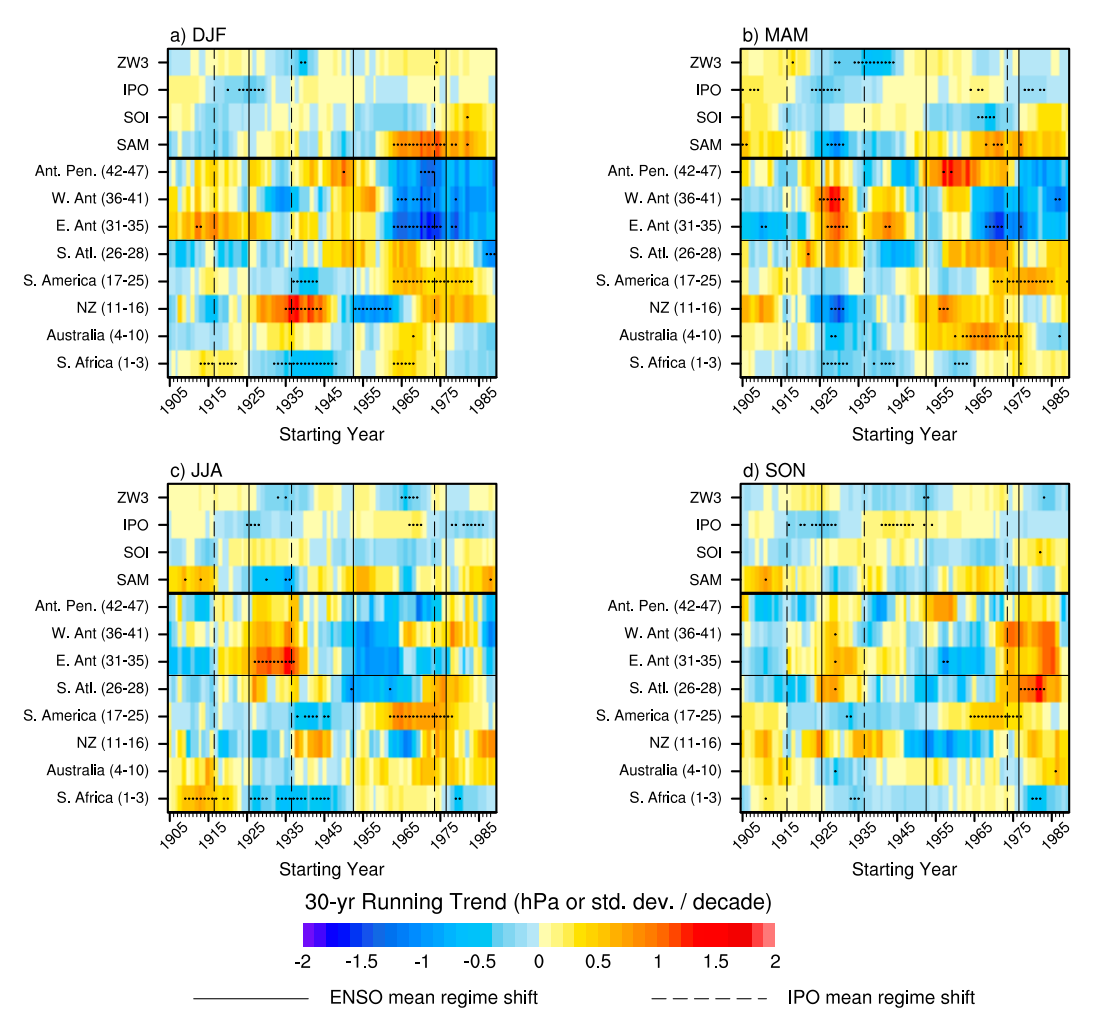


FIG. 6. The 30-yr running regionally averaged pressure trends along with the running trends in the seasonal mean major SH climate indices, as in Fig. 2, for (a) DJF, (b) MAM, (c) JJA, and (d) SON. The regional averaging is indicated by the *y*-axis labels, which include the station numbers from Fig. 1 where the averaging was performed. Thirty-year regionally averaged running trends that are significantly different from zero at p < 0.05 are marked with a dot. Vertical lines indicate where the SOI (for ENSO; solid line) or IPO index (dashed lines) 30-yr running trends averaged across all four seasons shifts signs and stays in the new phase for at least five years to indicate regime shifts in Pacific climate variability. The *x* axis is the starting year for the 30-yr running trend.

dominance of strong SOI positive events (La Niña events) from 1925 to 1940 and again after 1950, while strong SOI negative events (El Niño) primarily occur before 1920 and in the period from 1939 to 1949. Regionally, in DJF and JJA there are significant negative pressure anomalies across Africa in La Niña that are absent during El Niño (Fig. 7). In most seasons, the Antarctic Peninsula region shows negative pressure anomalies nearby in the South Pacific in La Niña years (Fig. 7, left column) and positive pressure anomalies in El Niño years. Some of these pressure anomalies near the Antarctic Peninsula are statistically significant; however, the lower reconstruction skill incorporated into the merged data in the high-latitude South Pacific (Fogt et al. 2019, 2020) likely limits the full depiction of this

signal. For the 1957–2013 period, the pressure anomalies during ENSO events are stronger near the Antarctic Peninsula (Fig. S3 of the online supplemental material). Similar shifts in pressure anomalies between ENSO phases are commonly seen across Australia and New Zealand (Jiang et al. 2013; Lorrey and Fauchereau 2018), consistent with some of the apparent, albeit weaker, relationships with the SOI and pressure trends in Fig. 6. These teleconnections prior to the IGY reflect the regional character of the Pacific–South American pattern emanating from the tropical Pacific, stretching toward the Antarctic Peninsula, and arching equatorward toward South Africa in the South Atlantic Ocean, largely missing much of South America (Karoly 1989; Mo and Paegle 2001; Turner 2004; Clem and Fogt 2013;

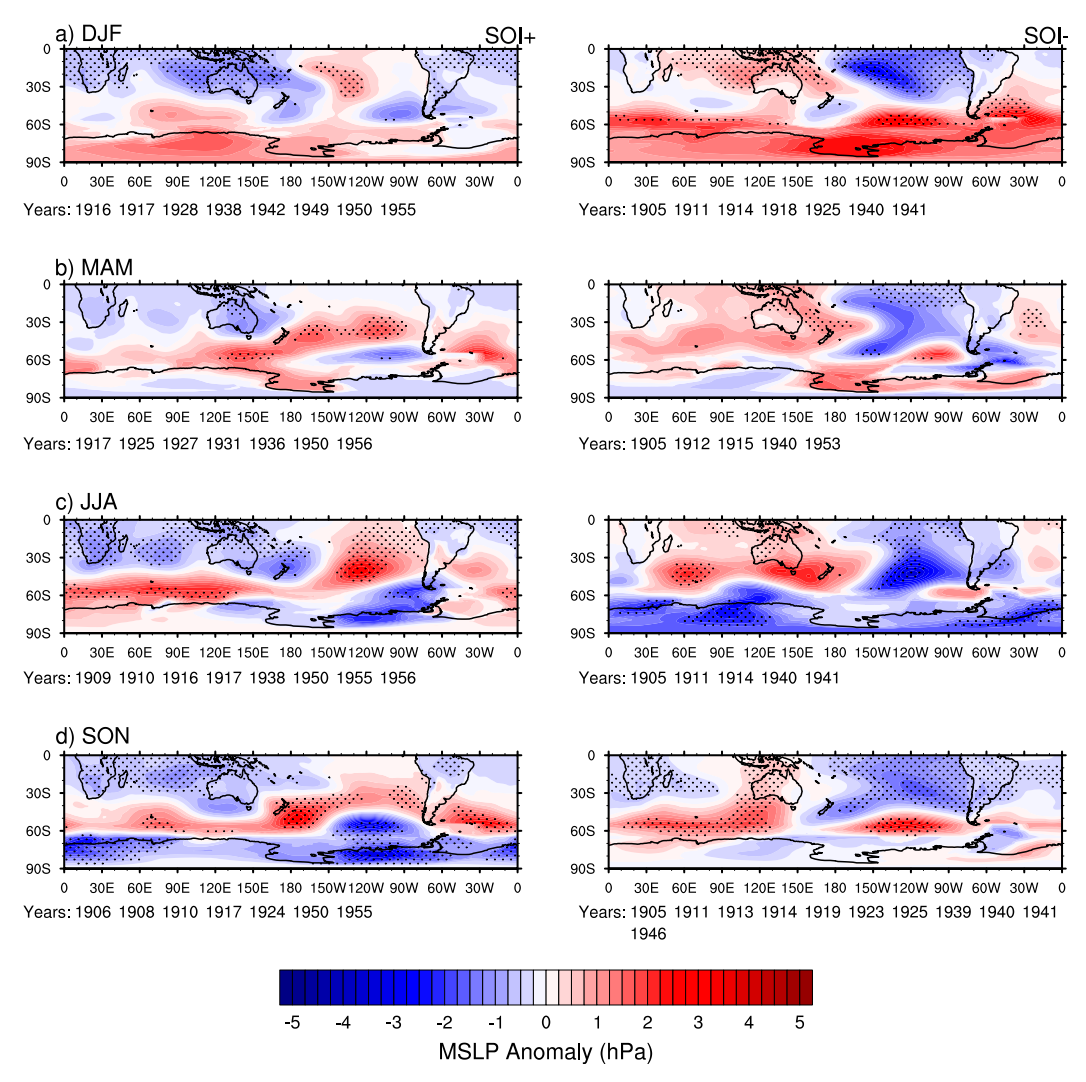


FIG. 7. Seasonal pressure anomaly composites from the merged dataset for (left) SOI+ and (right) SOI- years during 1905–56, for (a) DJF, (b) MAM, (c) JJA, and (d) SON. The pressure anomalies are relative to the 1905–99 seasonal mean. The years included in the composites are given beneath each map; years were selected for which the SOI was at least  $\pm 1$  standard deviation from its 1905–99 mean for each season. The stippling indicates pressure anomalies that are statistically different from zero at p < 0.05.

Clem et al. 2016; Yuan et al. 2018), consistent with the weak relationship with ENSO there (Figs. 6 and 7). The new analysis presented here using the merged data suggests that these regional connections remain throughout the early twentieth century prior to the IGY.

#### 2) RELATIONSHIPS WITH THE IPO RESIDUAL

Relative to both SAM and ENSO, the relationships between SH extratropical pressure variability with the IPO residual, when regionally averaged, are much weaker (Fig. 6). The residual IPO index has three regime shifts based on the method employed here, occurring in 1916/17 (from positive running trends to negative), 1936/37 (negative running trends to positive), and 1973/74. Over the entire time period represented in Fig. 6, the strongest association of the IPO and pressure trends

across the extratropical SH is across the southern Atlantic Ocean (stations 26–28) outside of austral summer since the 1936/37 regime shift (Figs. 6b,c,d). The composites for the IPO phases independent of ENSO (Fig. 8) show significant positive pressure anomalies across much of the southern Atlantic Ocean during the negative IPO phases that are generally absent in positive IPO phases, reflecting some of the IPO associations depicted in Fig. 6. Importantly, the relationship with the IPO and southern Atlantic Ocean pressure trends in Fig. 6 is strongest after the IGY, reflected as an (absolute) intensification of many of the high-latitude pressure anomalies in the IPO composites during 1957–2013 (Fig. S4 of the online supplemental material). Hence, SH extratropical pressure relationships with the IPO may be weaker in the early twentieth century, or they may not be well represented in the composites

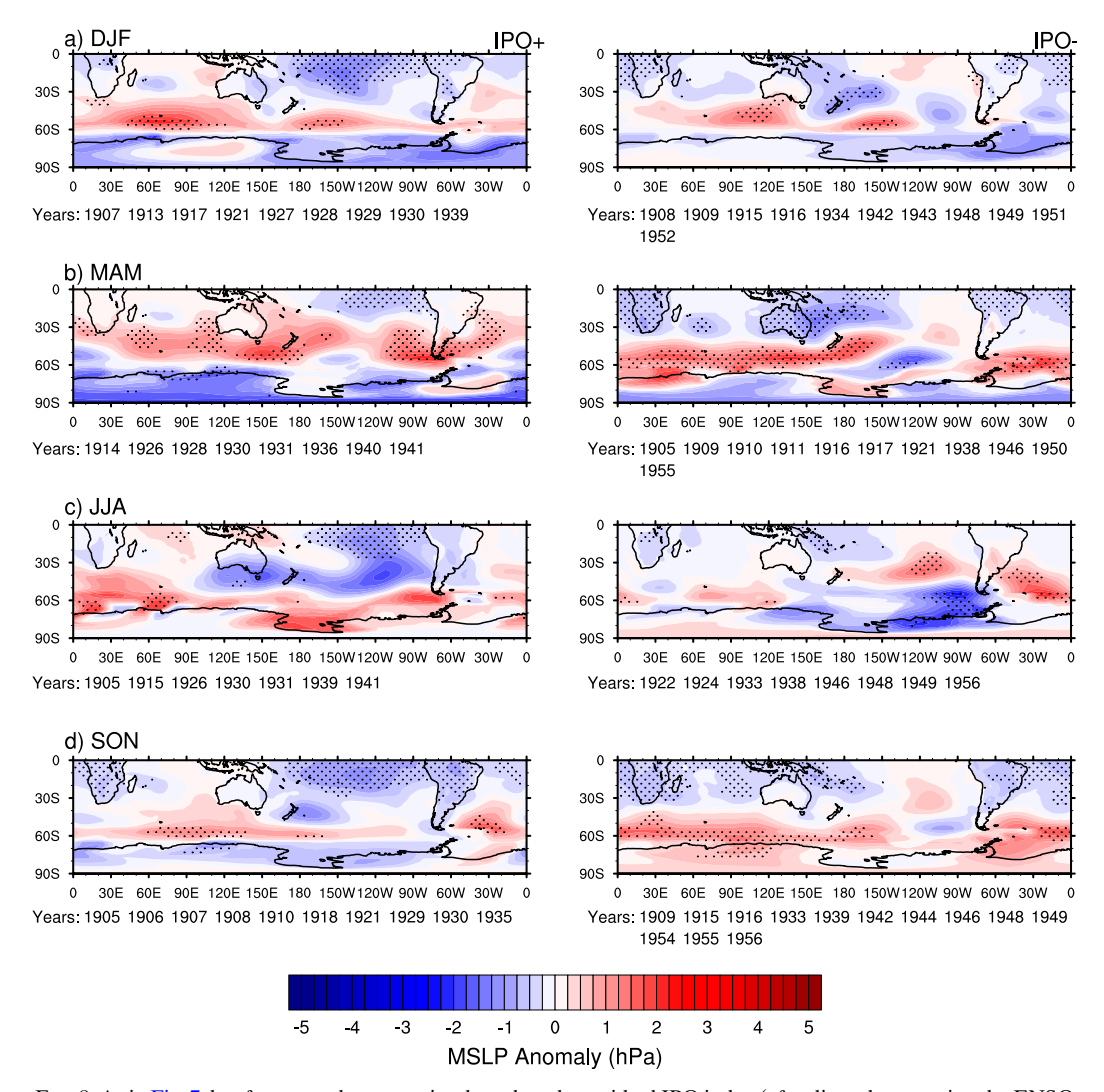


FIG. 8. As in Fig. 7, but for anomaly composites based on the residual IPO index (after linearly removing the ENSO signal from the IPO index).

due to uncertainties in the merged data in the southern Atlantic Ocean. Given that there are a few observations in the southern Atlantic Ocean in the early twentieth century (stations 26–28 in Fig. 1), the former seems likely, but further research is warranted to document such changes in the IPO teleconnections throughout the twentieth century.

Apart from the robust teleconnection in the southern Atlantic Ocean, Fig. 8 hints at a few other possible pressure relationships with the IPO prior to the IGY, although these are admittedly much weaker than for ENSO and the SAM, and statistically significant pressure anomalies primarily occur over the ocean. Over Antarctica, the relationship of pressure variations with the IPO appears the strongest in JJA and SON (Figs. 6 and 8); in JJA pressure anomalies weaken over much of Antarctica in the period 1957–2013 (Fig. S4). Although largely nonsignificant, shifts in the IPO index running trends (vertical dashed lines in Fig. 6) broadly align with some of the shifts of the signs of Antarctic 30-yr running pressure trends in austral winter and spring. In

particular, there is a clear shift between the IPO phases and the sign of the pressure anomalies across Antarctica in JJA and SON. In JJA (Fig. 8c), positive pressure anomalies around 60°S stretching to Antarctica in IPO positive phases, some statistically significant, are replaced during IPO negative phases with negative pressure anomalies, some of which are also statistically significant. The large differences in pressure anomalies between IPO phases near West Antarctica are statistically significant during 1905–2013 (Fig. 8c). In SON, the IPO index shifts are even more impressive, with statistically significant (p < 0.05) negative 30-yr running trends for the 30-yr periods beginning in 1915–30, becoming statistically significant positive running trends for the 30-yr periods beginning in 1940-50. Although the composites do not show significant pressure anomalies across Antarctica in SON during 1905–2013 (Fig. 8d), the running pressure trends across Antarctica, except over the Antarctic Peninsula, in SON are loosely connected with these IPO shifts (vertical dashed lines in Fig. 6d) and more statistically significant pressure anomalies in

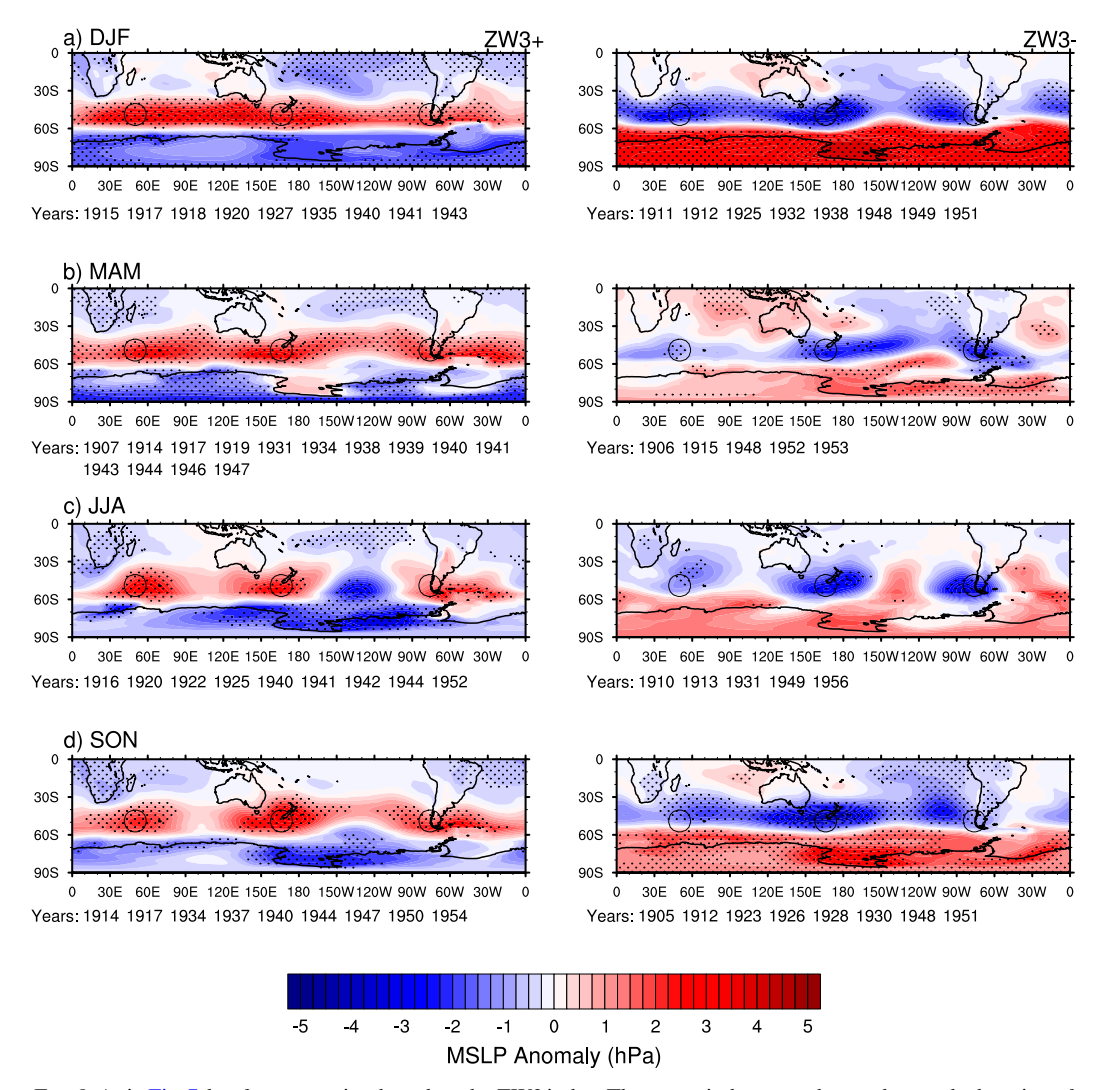


FIG. 9. As in Fig. 7, but for composites based on the ZW3 index. The open circles on each map denote the location of the ZW3 centers used to create the ZW3 index from Raphael (2004).

SON are found in the IPO composites after 1957 (Fig. S4). Specifically, the large region labeled "West Antarctica" (stations 36–41 in Fig. 1; Vostok-Byrd) is generally characterized by negative pressure trends prior to the 1916/17 IPO regime shift, positive pressure trends prior to the 1936/37 regime shift, and strong positive trends after the 1973/74 IPO regime shift (Fig. 6d). The IPO pressure associations are reflected also in East Antarctica, with a few statistically significant pressure trends. Figures 6 and 8 suggest that over Antarctica, especially in West Antarctica and the southern Atlantic Ocean, strong associations of the IPO with regional climate since 1979, including sea ice extent and temperature trends (Nicolas and Bromwich 2014; Clem and Fogt 2015; Meehl et al. 2016; Purich and England 2019), have occurred at other times prior to the IGY.

### 3) RELATIONSHIPS WITH ZONAL WAVENUMBER 3

From Fig. 6, there is a notable association between the ZW3 index of Raphael (2004) with the SAM throughout the

twentieth century. The ZW3 composites also reflect this relationship, with ZW3 positive phases showing pressure anomalies similar to positive SAM phases, and ZW3 negative phases showing pressure anomalies similar to negative SAM phases both prior to the IGY (Fig. 9) and after the IGY (Fig. S5 of the online supplemental material) (Fogt and Marshall 2020). However, the zonal symmetry in the Z3 composites is much weaker in JJA and SON, especially in the midlatitudes, while the SAM composites (Figs. S1 and S2) continue to show nearly uniform (but opposite) pressure anomalies across both the midlatitudes and Antarctica in all seasons. Nonetheless, due to the location of the Rossby wave centers used to define the ZW3 index at 49°S (depicted as open circles in Fig. 9), the teleconnections are robust across New Zealand (Jiang et al. 2013), as well as southern South America, and exist throughout the twentieth century. The teleconnections with South America are not clear in Fig. 6 due to averaging over a much larger region than southern South America, where the statistically

significant pressure anomalies associated with ZW3 occur both prior to the IGY (Fig. 9) and after the IGY (Fig. S5). Consistent with the seasonally varying structure of the SAM (Fogt et al. 2012; Fogt and Marshall 2020) and the known seasonal intensification of the Rossby waves associated with the ZW3 pattern (Raphael 2004), the ZW3 composites prior to the IGY (Fig. 9) show a much more pronounced meridional structure in JJA and SON, as alluded to earlier. In the Ross Sea region, there are distinctly different pressure anomalies in JJA and SON between the ZW3 phases (Figs. 9c,d); these are not fully captured in Fig. 6 due to the large area averaging for stations 36-41 (Fig. 1) and the more regional character of the pressure anomalies across the Ross Sea region in Figs. 9c,d. One notable feature of the ZW3 that is independent from the SAM is the long period of statistically significant negative ZW3 index trends for 30-yr periods beginning in 1930-40 in MAM (Fig. 6b). These significant negative ZW3 trends in MAM are likely linked to at least a portion of the statistically significant negative pressure trends across southern Africa and positive pressure trends across East Antarctica at this time (Fig. 6b). Spatially, a deep trough in negative ZW3 phases situated over the Indian Ocean center of the ZW3 in MAM (Fig. 9b, right column) with opposing pressure anomalies across East Antarctica and pressure trend changes across southern Africa (Fig. 6b) reflect the changes in the ZW3 during 1930–60 (Fig. 6b).

#### 4. Summary and conclusions

The goal of this work was to explore pressure relationships across the extratropical SH throughout the twentieth century that were previously difficult to establish due to problems with data quality across Antarctica in the early twentieth century prior to the IGY of 1957–58 (Schneider and Fogt 2018). Given that multiple evaluations with independent data have demonstrated the skill of pressure reconstructions across Antarctica (Fogt et al. 2016a, 2019, 2020), the focus of this work was primarily in the early twentieth century prior to the IGY to expand upon well-established teleconnections after 1979 using global reanalyses.

Throughout the early twentieth century, pressure increases at many of the Antarctic stations are balanced by decreases in pressure at many midlatitude stations, especially in DJF and MAM. On SH landmasses, the strongest synchronous pressure variability occurs between Australia and New Zealand and much of Antarctica, except for the Antarctic Peninsula, which is different from previous studies that have focused on the TPI. In the Antarctic Peninsula and even in much of South America, more regional and temporally varying pressure trends have been observed throughout the early twentieth century, including their teleconnections between the middle and high latitudes. In general, these relationships are not observed in gridded twentieth-century reanalyses due to large statistically significant trends that do not match the Antarctic station-based pressure reconstructions.

Most of the synchronous pressure variability prior to the IGY is consistent with the SAM index (and EOF1), extending its known effects back farther in time. Shifts in the sign of running trends of the SAM index prior to 1950 are often

associated with simultaneous, but opposite, shifts in the sign of pressure trends between Antarctica and the SH midlatitudes. However, tropical variability also plays an important role in synchronous SH pressure variability prior to the IGY, much like it plays an important role in Antarctic climate variability since 1979 (Ding et al. 2011; Ding and Steig 2013; Clem and Fogt 2015; Meehl et al. 2016; Yuan et al. 2018; Purich and England 2019). In particular, regime shifts in ENSO accompany regional pressure anomalies from Australia/New Zealand through the Antarctica Peninsula and extending equatorward to south Africa prior to the middle of the twentieth century based on a spatially continuous pressure dataset analyzed here. The analysis also suggests that pressure anomalies since the 1950s across the southern Atlantic are largely associated with the IPO, whereas there was likely a deeper trough in the southern Indian Ocean in MAM during the 1940s associated with a node of the zonal wavenumber 3 pattern. The new spatially complete analysis presented here suggests that a larger portion of synchronous pressure variability connecting the SH middle and high latitudes in austral winter and spring occurs independent of the SAM prior to the IGY; the more regional character of the synchronous SH extratropical pressure variability, particularly in austral winter and spring, is associated with the stronger tropical teleconnections that emerge across the SH outside of austral summer.

Although the relationships established here are based primarily on trends and anomaly composites, they suggest that many of the known relationships between Antarctica and the southern midlatitudes exist throughout the early twentieth century prior to Antarctic observations beginning in the IGY. It is critical to note that work establishing these associations in data-sparse regions like the SH high latitudes prior to the IGY would not be possible without the considerable efforts in historical data rescue from nonconventional sources. One such project, the Atmospheric Reconstructions over Earth (ACRE), has aided significantly in this regard, especially for historical observations obtained from early expeditions and ship logbooks in and around Antarctica (Allan et al. 2011). Relevant to the present study, the efforts accomplished through ACRE have dramatically improved the quality of the twentieth-century reanalyses and have made possible the creation of the merged data employed here. With the new knowledge gained from ACRE and similar initiatives, it is hoped that future research can be inspired to detail the dynamics and more precisely attribute climate trends in datasparse regions like the extratropical SH. Ultimately, such work would better place historical and future climate trends across the extratropical SH in a more spatially complete and temporally continuous context. A longer and more spatially complete historical context for SH climate is especially important given some of the rapid trends in Antarctic climate in sea ice, temperature, and atmospheric circulation seen since the late twentieth century (Paolo et al. 2015; Jones et al. 2016; Banerjee et al. 2020; Turner et al. 2020).

Acknowledgments. This paper extends the research from the undergraduate honors thesis of author C. Connolly. Authors Fogt and Connolly acknowledge support from the National Science Foundation (NSF), ANT-1744998.

Data availability statement. Data from both the station-based and spatial pressure reconstructions are available online from figshare at https://doi.org/10.6084/m9.figshare.3412813 (station reconstructions) and https://doi.org/10.6084/m9.figshare.5325541 (spatial reconstructions).

#### REFERENCES

- Abram, N. J., R. Mulvaney, F. Vimeux, S. J. Phipps, J. Turner, and M. H. England, 2014: Evolution of the Southern Annular Mode during the past millennium. *Nat. Climate Change*, 4, 564–569, https://doi.org/10.1038/nclimate2235.
- Alexander, L. V., P. Uotila, N. Nicholls, and A. Lynch, 2010: A new daily pressure dataset for Australia and its application to the assessment of changes in synoptic patterns during the last century. J. Climate, 23, 1111–1126, https://doi.org/10.1175/ 2009JCLI2972.1.
- Allan, R., N. Nicholls, P. D. Jones, and I. J. Butterworth, 1991: A further extension of the Tahiti-Darwin SOI, early ENSO events and Darwin pressure. *J. Climate*, 4, 743–749, https://doi.org/ 10.1175/1520-0442(1991)004<0743:AFEOTT>2.0.CO;2.
- —, J. A. Lindesay, and C. J. C. Reason, 1995: Multidecadal variability in the climate system over the Indian Ocean region during the austral summer. *J. Climate*, 8, 1853–1873, https://doi.org/10.1175/1520-0442(1995)008<1853:MVITCS>2.0.CO;2.
- —, P. Brohan, G. P. Compo, R. Stone, J. Luterbacher, and S. Brönnimann, 2011: The international Atmospheric Circulation Reconstructions over the Earth (ACRE) initiative. *Bull. Amer. Meteor. Soc.*, **92**, 1421–1425, https://doi.org/10.1175/2011BAMS3218.1.
- Bals-Elsholz, T. M., E. H. Atallah, L. F. Bosart, T. A. Wasula, M. J. Cempa, and A. R. Lupo, 2001: The wintertime Southern Hemisphere split jet: Structure, variability, and evolution. J. Climate, 14, 4191–4215, https://doi.org/10.1175/1520-0442(2001)014<4191:TWSHSJ>2.0.CO;2.
- Banerjee, A., J. C. Fyfe, L. M. Polvani, D. Waugh, and K.-L. Chang, 2020: A pause in Southern Hemisphere circulation trends due to the Montreal protocol. *Nature*, 579, 544–548, https://doi.org/10.1038/s41586-020-2120-4.
- Bracegirdle, T. J., and Coauthors, 2019: Back to the future: Using long-term observational and paleo-proxy reconstructions to improve model projections of Antarctic climate. *Geosciences*, 9, 255, https://doi.org/10.3390/geosciences9060255.
- Bretherton, C. S., M. Widmann, V. P. Dymnikov, J. M. Wallace, and I. Bladé, 1999: The effective number of spatial degrees of freedom of a time-varying field. *J. Climate*, **12**, 1990–2009, https://doi.org/10.1175/1520-0442(1999)012<1990: TENOSD>2.0.CO;2.
- Carleton, A. M., 2003: Atmospheric teleconnections involving the Southern Ocean. J. Geophys. Res., 108, 8080, https://doi.org/ 10.1029/2000JC000379.
- Clark, L., and R. L. Fogt, 2019: Southern Hemisphere pressure relationships during the 20th century—Implications for climate reconstructions and model evaluation. *Geosciences*, 9, 413, https://doi.org/10.3390/geosciences9100413.
- Clem, K. R., and R. L. Fogt, 2013: Varying roles of ENSO and SAM on the Antarctic Peninsula climate in austral spring. *J. Geophys. Res. Atmos.*, 118, 11 481–11 492, https://doi.org/ 10.1002/jgrd.50860.
- —, and —, 2015: South Pacific circulation changes and their connection to the tropics and regional Antarctic warming in austral spring, 1979–2012. *J. Geophys. Res. Atmos.*, **120**, 2773–2792, https://doi.org/10.1002/2014JD022940.

- —, J. A. Renwick, J. McGregor, and R. L. Fogt, 2016: The relative influence of ENSO and SAM on Antarctic Peninsula climate. *J. Geophys. Res. Atmos.*, **121**, 9324–9341, https://doi.org/10.1002/2016JD025305.
- Dätwyler, C., R. Neukom, N. J. Abram, A. J. E. Gallant, M. Grosjean, M. Jacques-Coper, D. J. Karoly, and R. Villalba, 2018: Teleconnection stationarity, variability and trends of the Southern Annular Mode (SAM) during the last millennium. Climate Dyn., 51, 2321–2339, https://doi.org/10.1007/s00382-017-4015-0.
- Ding, Q., and E. J. Steig, 2013: Temperature change on the Antarctic Peninsula linked to the tropical Pacific. *J. Climate*, **26**, 7570–7585, https://doi.org/10.1175/JCLI-D-12-00729.1.
- ——, D. S. Battisti, and M. Küttel, 2011: Winter warming in West Antarctica caused by central tropical Pacific warming. *Nat. Geosci.*, 4, 398–403, https://doi.org/10.1038/ngeo1129.
- Dixon, D. A., P. A. Mayewski, I. D. Goodwin, G. J. Marshall, R. Freeman, K. A. Maasch, and S. B. Sneed, 2012: An icecore proxy for northerly air mass incursions into West Antarctica. *Int. J. Climatol.*, 32, 1455–1465, https://doi.org/ 10.1002/joc.2371.
- Enomoto, H., 1991: Fluctuations of snow accumulation in the Antarctic and sea level pressure in the Southern Hemisphere in the last 100 years. *Climatic Change*, **18**, 67–87, https://doi.org/10.1007/BF00142505.
- Fogt, R. L., and D. H. Bromwich, 2006: Decadal variability of the ENSO teleconnection to the high-latitude South Pacific governed by coupling with the southern annular mode. *J. Climate*, **19**, 979–997, https://doi.org/10.1175/JCLI3671.1.
- —, and G. J. Marshall, 2020: The southern annular mode: Variability, trends, and climate impacts across the Southern Hemisphere. Wiley Interdiscip. Rev.: Climate Change, 11, e652, https://doi.org/10.1002/wcc.652.
- —, J. Perlwitz, A. J. Monaghan, D. H. Bromwich, J. M. Jones, and G. J. Marshall, 2009: Historical SAM variability. Part II: Twentieth-century variability and trends from reconstructions, observations, and the IPCC AR4 models. J. Climate, 22, 5346–5365, https://doi.org/10.1175/2009JCL12786.1.
- —, J. M. Jones, and J. Renwick, 2012: Seasonal zonal asymmetries in the southern annular mode and their impact on regional temperature anomalies. *J. Climate*, 25, 6253–6270, https://doi.org/10.1175/JCLI-D-11-00474.1.
- —, C. A. Goergens, M. E. Jones, G. A. Witte, M. Y. Lee, and J. M. Jones, 2016a: Antarctic station-based seasonal pressure reconstructions since 1905: 1. Reconstruction evaluation. *J. Geophys. Res. Atmos.*, 121, 2814–2835, https://doi.org/10.1002/ 2015JD024564.
- —, J. M. Jones, C. A. Goergens, M. E. Jones, G. A. Witte, and M. Y. Lee, 2016b: Antarctic station-based seasonal pressure reconstructions since 1905: 2. Variability and trends during the twentieth century. *J. Geophys. Res. Atmos.*, **121**, 2836–2856, https://doi.org/10.1002/2015JD024565.
- —, C. A. Goergens, J. M. Jones, D. P. Schneider, J. P. Nicolas, D. H. Bromwich, and H. E. Dusselier, 2017: A twentieth century perspective on summer Antarctic pressure change and variability and contributions from tropical SSTs and ozone depletion. *Geophys. Res. Lett.*, 44, 9918–9927, https://doi.org/10.1002/2017GL075079.
- —, L. N. Clark, and J. P. Nicolas, 2018: A new monthly pressure dataset poleward of 60°S since 1957. J. Climate, 31, 3865–3874, https://doi.org/10.1175/JCLI-D-17-0879.1.
- —, D. P. Schneider, C. A. Goergens, J. M. Jones, L. N. Clark, and M. J. Garberoglio, 2019: Seasonal Antarctic pressure variability

- during the twentieth century from spatially complete reconstructions and CAM5 simulations. *Climate Dyn.*, **53**, 1435–1452, https://doi.org/10.1007/s00382-019-04674-8.
- —, C. P. Belak, J. M. Jones, L. C. Slivinski, and G. P. Compo, 2020: An Assessment of early 20th century Antarctic pressure reconstructions using historical observations. *Int. J. Climatol.*, 41, E672–E689, https://doi.org/10.1002/joc.6718.
- Gillett, N. P., T. D. Kell, and P. D. Jones, 2006: Regional climate impacts of the Southern Annular Mode. *Geophys. Res. Lett.*, 33, L23704, https://doi.org/10.1029/2006GL027721.
- Goodwin, I. D., T. D. van Ommen, M. A. J. Curran, and P. A. Mayewski, 2004: Mid latitude winter climate variability in the South Indian and southwest Pacific regions since 1300 AD. *Climate Dyn.*, 22, 783–794, https://doi.org/10.1007/s00382-004-0403-3.
- Henley, B. J., J. Gergis, D. J. Karoly, S. Power, J. Kennedy, and C. K. Folland, 2015: A tripole index for the Interdecadal Pacific Oscillation. *Climate Dyn.*, 45, 3077–3090, https://doi.org/10.1007/s00382-015-2525-1.
- Jiang, N., G. Griffiths, and A. Lorrey, 2013: Influence of large-scale climate modes on daily synoptic weather types over New Zealand. *Int. J. Climatol.*, 33, 499–519, https://doi.org/10.1002/joc.3443.
- Jones, J. M., and M. Widmann, 2003: Instrument- and tree-ring-based estimates of the Antarctic oscillation. *J. Climate*, 16, 3511–3524, https://doi.org/10.1175/1520-0442(2003)016<3511: IATEOT>2.0.CO;2.
- —, and —, 2004: Early peak in Antarctic oscillation index. *Nature*, **432**, 290–291, https://doi.org/10.1038/432290b.
- ——, R. L. Fogt, M. Widmann, G. J. Marshall, P. D. Jones, and M. Visbeck, 2009: Historical SAM variability. Part I: Centurylength seasonal reconstructions. *J. Climate*, 22, 5319–5345, https://doi.org/10.1175/2009JCLI2785.1.
- —, and Coauthors, 2016: Assessing recent trends in high-latitude Southern Hemisphere surface climate. *Nat. Climate Change*, **6**, 917–926, https://doi.org/10.1038/nclimate3103.
- Jones, P. D., 1991: Southern Hemisphere sea-level pressure data: An analysis and reconstructions back to 1951 and 1911. Int. J. Climatol., 11, 585–607, https://doi.org/10.1002/joc.3370110603.
- —, and T. M. L. Wigley, 1988: Antarctic gridded sea level pressure data: An analysis and reconstruction back to 1957.
  J. Climate, 1, 1199–1220, https://doi.org/10.1175/1520-0442(1988) 001<1199:AGSLPD>2.0.CO;2.
- —, M. J. Salinger, and A. B. Mullan, 1999: Extratropical circulation indices in the Southern Hemisphere based on station data. Int. J. Climatol., 19, 1301–1317, https://doi.org/10.1002/(SICI) 1097-0088(199910)19:12<1301::AID-JOC425>3.0.CO;2-P.
- Karoly, D. J., 1989: Southern Hemisphere circulation features associated with El Niño–Southern Oscillation events. *J. Climate*, 2, 1239–1252, https://doi.org/10.1175/1520-0442(1989)002<1239: SHCFAW>2.0.CO;2.
- ——, P. Hope, and P. D. Jones, 1996: Decadal variations of the Southern Hemisphere circulation. *Int. J. Climatol.*, 16, 723–738, https://doi.org/10.1002/(SICI)1097-0088(199607)16: 7<723::AID-JOC54>3.0.CO;2-6.
- Kreutz, K. J., P. A. Mayewski, I. I. Pittalwala, L. D. Meeker, M. S. Twickler, and S. I. Whitlow, 2000: Sea level pressure variability in the Amundsen Sea region inferred from a West Antarctic glaciochemical record. *J. Geophys. Res. Atmos.*, 105, 4047–4059, https://doi.org/10.1029/1999JD901069.
- Laloyaux, P., and Coauthors, 2018: CERA-20C: A coupled reanalysis of the twentieth century. J. Adv. Model. Earth Syst., 10, 1172–1195, https://doi.org/10.1029/2018MS001273.

- Lorrey, A. M., and N. C. Fauchereau, 2018: Southwest Pacific atmospheric weather regimes: Linkages to ENSO and extratropical teleconnections. *Int. J. Climatol.*, 38, 1893–1909, https://doi.org/10.1002/joc.5304.
- Marshall, G. J., 2003: Trends in the southern annular mode from observations and reanalyses. *J. Climate*, **16**, 4134–4143, https://doi.org/10.1175/1520-0442(2003)016<4134: TITSAM>2.0.CO;2.
- Meehl, G. A., J. M. Arblaster, C. M. Bitz, C. T. Y. Chung, and H. Teng, 2016: Antarctic sea-ice expansion between 2000 and 2014 driven by tropical Pacific decadal climate variability. *Nat. Geosci.*, **9**, 590–595, https://doi.org/10.1038/ngeo2751.
- Mo, K. C., and J. N. Paegle, 2001: The Pacific–South American modes and their downstream effects. *Int. J. Climatol.*, 21, 1211–1229, https://doi.org/10.1002/joc.685.
- Nicolas, J. P., and D. H. Bromwich, 2014: New reconstruction of Antarctic near-surface temperatures: Multidecadal trends and reliability of global reanalyses. *J. Climate*, 27, 8070–8093, https://doi.org/10.1175/JCLI-D-13-00733.1.
- Paolo, F. S., H. A. Fricker, and L. Padman, 2015: Volume loss from Antarctic ice shelves is accelerating. *Science*, 348, 327–331, https://doi.org/10.1126/science.aaa0940.
- Pittock, A. B., 1980: Patterns of climatic variation in Argentina and Chile—I. Precipitation, 1931–60. *Mon. Wea. Rev.*, 108, 1347–1361, https://doi.org/10.1175/1520-0493(1980)108<1347: POCVIA>2.0.CO;2.
- Poli, P., and Coauthors, 2016: ERA-20C: An atmospheric reanalysis of the twentieth century. *J. Climate*, 29, 4083–4097, https://doi.org/10.1175/JCLI-D-15-0556.1.
- Polvani, L. M., D. W. Waugh, G. J. P. Correa, and S.-W. Son, 2011: Stratospheric ozone depletion: The main driver of twentiethcentury atmospheric circulation changes in the Southern Hemisphere. J. Climate, 24, 795–812, https://doi.org/10.1175/ 2010JCLI3772.1.
- Purich, A., and M. H. England, 2019: Tropical teleconnections to Antarctic sea ice during austral spring 2016 in coupled pacemaker experiments. *Geophys. Res. Lett.*, 46, 6848–6858, https://doi.org/10.1029/2019GL082671.
- Raphael, M. N., 2004: A zonal wave 3 index for the Southern Hemisphere. *Geophys. Res. Lett.*, **31**, https://doi.org/10.1029/2004GL020365.
- Rogers, J. C., and H. van Loon, 1982: Spatial variability of sea level pressure and 500 mb height anomalies over the Southern Hemisphere. *Mon. Wea. Rev.*, **110**, 1375–1392, https://doi.org/10.1175/1520-0493(1982)110<1375:SVOSLP>2.0.CO;2.
- Ropelewski, C. F., and P. D. Jones, 1987: An extension of the Tahiti–Darwin Southern Oscillation index. *Mon. Wea. Rev.*, **115**, 2161–2165, https://doi.org/10.1175/1520-0493(1987)115<2161: AEOTTS>2.0.CO;2.
- Russell, A., and G. R. McGregor, 2010: Southern Hemisphere atmospheric circulation: Impacts on Antarctic climate and reconstructions from Antarctic ice core data. *Climatic Change*, 99, 155–192, https://doi.org/10.1007/s10584-009-9673-4.
- Schneider, D. P., and R. L. Fogt, 2018: Artifacts in century-length atmospheric and coupled reanalyses over Antarctica due to historical data availability. *Geophys. Res. Lett.*, 45, 964–973, https://doi.org/10.1002/2017GL076226.
- Slivinski, L. C., and Coauthors, 2019: Towards a more reliable historical reanalysis: Improvements for version 3 of the Twentieth Century Reanalysis system. *Quart. J. Roy. Meteor. Soc.*, 145, 2876–2908, https://doi.org/10.1002/qj.3598.
- Souney, J. M., 2002: A 700-year record of atmospheric circulation developed from the Law Dome ice core, East

- Antarctica. J. Geophys. Res., 107, 4608, https://doi.org/10.1029/2002JD002104.
- Thompson, D. W. J., and J. M. Wallace, 2000: Annular modes in the extratropical circulation. Part I: Month-to-month variability. *J. Climate*, **13**, 1000–1016, https://doi.org/10.1175/1520-0442(2000)013<1000:AMITEC>2.0.CO;2.
- —, and S. Solomon, 2002: Interpretation of recent Southern Hemisphere climate change. *Science*, **296**, 895–899, https://doi.org/10.1126/science.1069270.
- Turner, J., 2004: The El Niño–Southern Oscillation and Antarctica. *Int. J. Climatol.*, **24**, 1–31, https://doi.org/10.1002/joc.965.
- —, and Coauthors, 2009: Non-annular atmospheric circulation change induced by stratospheric ozone depletion and its role in the recent increase of Antarctic sea ice extent. *Geophys. Res. Lett.*, 36, L08502, https://doi.org/10.1029/2009GL037524.
- —, and Coauthors, 2020: Recent decrease of summer sea ice in the Weddell Sea, Antarctica. *Geophys. Res. Lett.*, 47, e2020GL087127, https://doi.org/10.1029/2020GL087127.

- Villalba, R., E. R. Cook, R. D. D'Arrigo, G. C. Jacoby, P. D. Jones, M. J. Salinger, and J. Palmer, 1997: Sea-level pressure variability around Antarctica since A.D. 1750 inferred from sub-antarctic tree-ring records. *Climate Dyn.*, 13, 375–390, https://doi.org/10.1007/s003820050172.
- Xiao, C., P. A. Mayewski, D. Qin, M. Zhang, and Y. Yan, 2004: Sea level pressure variability over the southern Indian Ocean inferred from a glaciochemical record in Princess Elizabeth Land, East Antarctica. J. Geophys. Res., 109, D16101, https:// doi.org/10.1029/2003JD004065.
- Yuan, X., M. R. Kaplan, and M. A. Cane, 2018: The interconnected global climate system—A review of tropical–polar teleconnections. J. Climate, 31, 5765–5792, https://doi.org/10.1175/ JCLI-D-16-0637.1.
- Zazulie, N., M. Rusticucci, and S. Solomon, 2010: Changes in climate at high southern latitudes: A unique daily record at Orcadas spanning 1903–2008. J. Climate, 23, 189–196, https://doi.org/10.1175/2009JCLI3074.1.